

## **Supporting information**

### **Copper(I) metal azolate framework showing unusual coordination mode for 1,2,4-triazole derivative and photocatalytic activity**

**Bai-Qiao Song, Chao Qin\*, Yu-Teng Zhang, Xue-Song Wu, Kui-Zhan Shao and Zhong-Min Su\***

Institute of Functional Material Chemistry; Key Laboratory of Polyoxometalate  
Science of Ministry of Education, Northeast Normal University, Changchun, 130024  
Jilin, People's Republic of China; E-mail: [qinc703@nenu.edu.cn](mailto:qinc703@nenu.edu.cn),  
[zmsu@nenu.edu.cn](mailto:zmsu@nenu.edu.cn)

## S1. Materials and Measurements

Chemicals were purchased from commercial sources and used without further purification. Powder X-ray diffraction (PXRD) was carried out with an X-ray diffractometer of Rigaku, Rint 2000. The C, H, and N elemental analyses were conducted on a Perkin-Elmer 240C elemental analyzer. The FT-IR spectra were recorded from KBr pellets in the range 4000-400  $\text{cm}^{-1}$  on a Mattson Alpha-Centauri spectrometer. Thermogravimetric analyses (TGA) were carried out on a Perkin-Elmer TG-7 analyzer heated from room temperature to 800  $^{\circ}\text{C}$  at a ramp rate of 5  $^{\circ}\text{C}/\text{min}$  under nitrogen. The photoluminescence spectra were measured on a Perkin-Elmer FLS-920 spectrometer.

## S2. Synthesis

The ligand 4-amino-3,5-bis(4-imidazol-1-ylphenyl)-1,2,4-triazole ( $\text{NH}_2\text{-L}$ ) was prepared following the method as described in the literature.<sup>1</sup>

**[Cu<sub>5</sub>L<sub>3</sub>(CN)<sub>2</sub>] $\cdot$ 6H<sub>2</sub>O (1):** A solid mixture of  $\text{NH}_2\text{-L}$  (37 mg, 0.1 mmol),  $\text{Cu}(\text{NO}_3)_2\cdot 3\text{H}_2\text{O}$  (100 mg, 0.41 mmol) was suspended in  $\text{H}_2\text{O}$  (6 ml) in a 15 ml Teflon-lined stainless steel container, then aqueous ammonia (28%, 2 mL) was added and the mixture was stirred in the air for 30 min. Finally, the container was tightly capped and put in an oven to heat at 180  $^{\circ}\text{C}$  for 72 h. The resulting yellowish block crystals were filtered, washed, and dried in air; Yield: *ca.* 62% based on 1 mol of  $\text{NH}_2\text{-L}$ . Elemental analysis calcd (%) for **1**  $\text{C}_{62}\text{H}_{54}\text{Cu}_5\text{N}_{23}\text{O}_6$  (1534.98): C 48.51, H 3.55, N 20.99%; found: C 49.90, H 3.11, N 21.73%. IR ( $\text{cm}^{-1}$ ): 3381(m), 3122(m), 2098(s), 1611(s), 1582(s), 1531(w), 1493(w), 1435(m), 1302(w), 1262(m), 1193(s), 1109(s), 1060(w), 1008(s), 993(s), 961(s), 834(m), 759(m), 727(m), 653(m), 620(s), 530(m).

## S4. Photocatalytic degradation experiments

The photochemical experiment was performed in a 250mL Pyrex reactor with the corresponding light source.  $\text{H}_2\text{O}_2$  (1.5 mmol/L, 1 mL) and powder of compound **1** (100 mg) were added to the RB solution (10 mg/L, pH = 7-8) with continuous shaking at room temperature. The photocatalytic experiments were carried out under

ultraviolet light ( $\lambda < 420$  nm) and visible light ( $\lambda > 420$  nm) irradiation with regular intervals, respectively. The photocatalytic activities were monitored by UV–vis measurements of the absorbency of the solution with a Lambda35 spectrophotometer (Perkin–Elmer, USA) after given time intervals. The decolorization rate of RB solution was calculated by the following formula:

$$D = (A_0 - A_1) / A_0 \times 100\%$$

where  $D$  is decolorization rate,  $A_0$  and  $A_1$  are the characteristic absorbency of RB solutions in adsorption equilibrium before and after irradiation, respectively.

#### **S4. X-ray crystallography**

Single-crystal X-ray diffraction data were recorded on a Bruker Apex CCD diffractometer with graphite-monochromated MoK $\alpha$  radiation ( $\lambda = 0.71069$  Å) at 293K. Absorption corrections were applied using multi-scan technique. All the structures were solved by Direct Method of SHELXS-97<sup>2</sup> and refined by full-matrix least-squares techniques using the SHELXL-97 program<sup>3</sup> within WINGX.<sup>4</sup> Non-hydrogen atoms were refined with anisotropic temperature parameters. H atoms bound to C and N were placed at calculated positions, refined as riders, and assigned  $U(\text{iso}) = 1.2 U(\text{eq})$  of their respective parent atoms. The water hydrogen positions were deduced from difference electron density map and the possibility of H-bonding. The detailed crystallographic data and structure refinement parameters for **1** are summarized in Table S1. Crystallographic data for the structure reported in this paper have also been deposited with the CCDC as deposition no. CCDC 1032259 (available free of charge, on application to the CCDC, 12 Union Rd., Cambridge CB2 1EZ, U.K.; e-mail [deposit@ccdc.cam.ac.uk](mailto:deposit@ccdc.cam.ac.uk)).

**Table S1.** Crystal data and structure refinements for compound **1**

Compound reference	<b>1</b>
Chemical formula	C <sub>62</sub> H <sub>46</sub> Cu <sub>5</sub> N <sub>23</sub> O <sub>2</sub>
Formula Mass	1534.98
Crystal system	Tetragonal
<i>a</i> /(Å)	20.777(5)
<i>b</i> /(Å)	20.777(5)
<i>c</i> /(Å)	13.715(5)
$\alpha$ /°	90
$\beta$ /°	90
$\gamma$ /°	90
Unit cell volume/(Å) <sup>3</sup>	5921(3)
Temperature/K	293(2)
Space group	<i>P4<sub>2</sub>/nmc</i>
No. of formula units per unit cell, <i>Z</i>	4
No. of reflections measured	32580
No. of independent reflections	2754
<i>R</i> <sub>int</sub>	0.0528
Final <i>R</i> <sub>1</sub> values ( <i>I</i> > 2σ( <i>I</i> )) <sup>a</sup>	0.0772
Final <i>wR</i> ( <i>F</i> <sup>2</sup> ) values ( <i>I</i> > 2σ( <i>I</i> )) <sup>b</sup>	0.1875
Final <i>R</i> <sub>1</sub> values (all data)	0.0944
Final <i>wR</i> ( <i>F</i> <sup>2</sup> ) values (all data)	0.1995
Goodness of fit on <i>F</i> <sup>2</sup>	1.004

<sup>a</sup> $R_1 = \sum ||F_o| - |F_c|| / \sum |F_o|$ . <sup>b</sup> $wR_2 = \sqrt{\sum w(|F_o|^2 - |F_c|^2)|^2} / \sum w(F_o^2)^{1/2}$

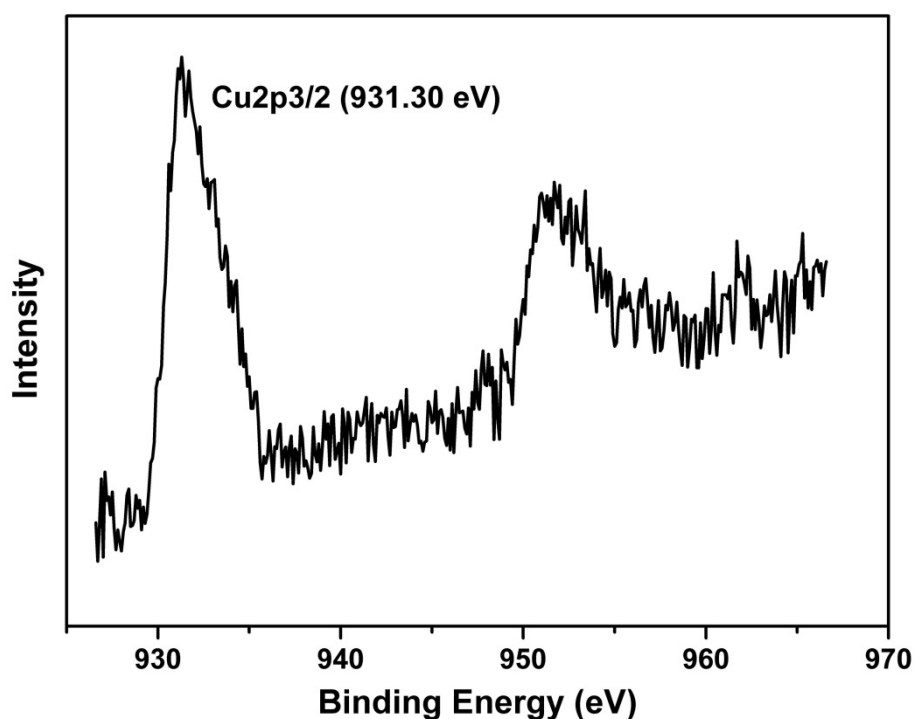
**Table S2. Selected bond lengths (Å) and bond angles (°)**

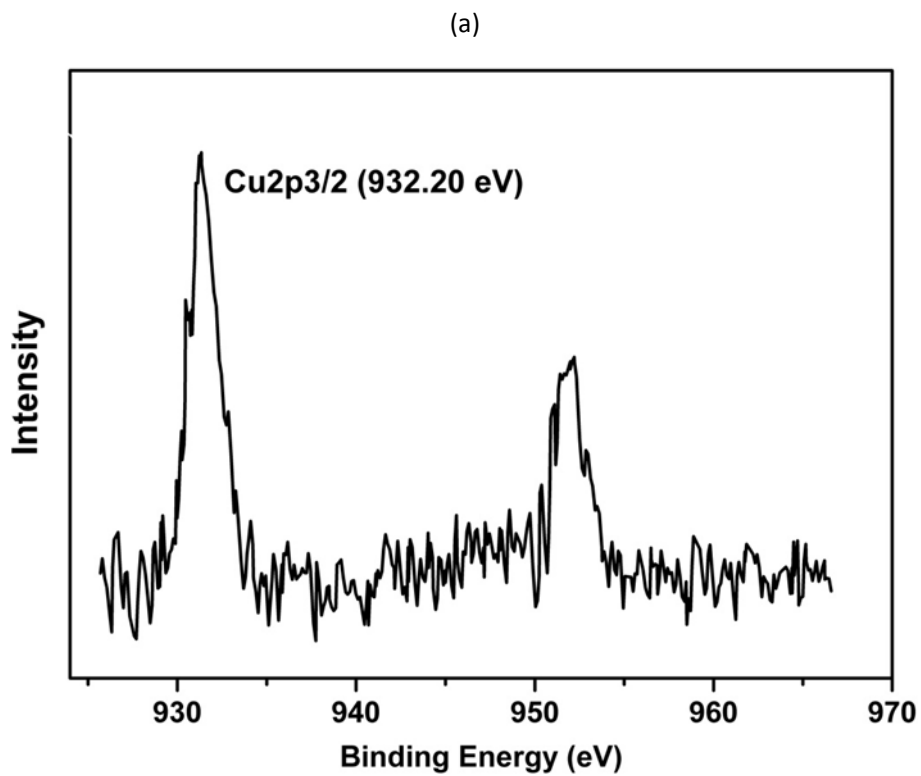
Bond lengths (Å)			
Cu(1)-N(1)#1	1.999(15)	Cu(2)-N(3)	2.039(6)
Cu(1)-N(1)	1.999(15)	Cu(3)-N(5)#3	1.938(5)
Cu(1)-N(7)	2.115(12)	Cu(3)-N(5)	1.938(5)
Cu(1)-N(7)#1	2.115(12)	Cu(3)-N(6)#3	2.382(6)
Cu(2)-C(21)	1.872(13)	Cu(3)-N(6)	2.382(6)
Cu(2)-N(3)#2	2.039(6)	N(6)-Cu(3)#5	2.382(6)

Bond angles (°)			
N(1)#1-Cu(1)-N(1)	126.7(9)	N(5)#3-Cu(3)-N(6)	107.0(2)
N(1)#1-Cu(1)-N(7)	103.3(3)	N(5)-Cu(3)-N(6)	93.6(2)
N(1)-Cu(1)-N(7)	103.3(3)	N(6)#3-Cu(3)-N(6)	91.3(4)
N(1)#1-Cu(1)-N(7)#1	103.3(3)	C(21)-N(1)-Cu(1)	162.6(16)
N(1)-Cu(1)-N(7)#1	103.3(3)	C(1)-N(3)-Cu(2)	120.3(6)
N(7)-Cu(1)-N(7)#1	118.2(7)	C(2)-N(3)-Cu(2)	131.7(5)
C(21)-Cu(2)-N(3)#2	118.4(2)	C(10)-N(5)-Cu(3)	138.0(4)
C(21)-Cu(2)-N(3)	118.4(2)	C(20)-N(6)-Cu(3)#5	124.8(4)
N(3)#2-Cu(2)-N(3)	112.8(4)	Cu(3)#5-N(6)-Cu(3)	79.6(3)
N(5)#3-Cu(3)-N(5)	150.6(3)	C(12)-N(7)-Cu(1)	140.9(19)
N(5)#3-Cu(3)-N(6)#3	93.6(2)	C(11)-N(7)-Cu(1)	112.8(10)
N(5)-Cu(3)-N(6)#3	107.0(2)		

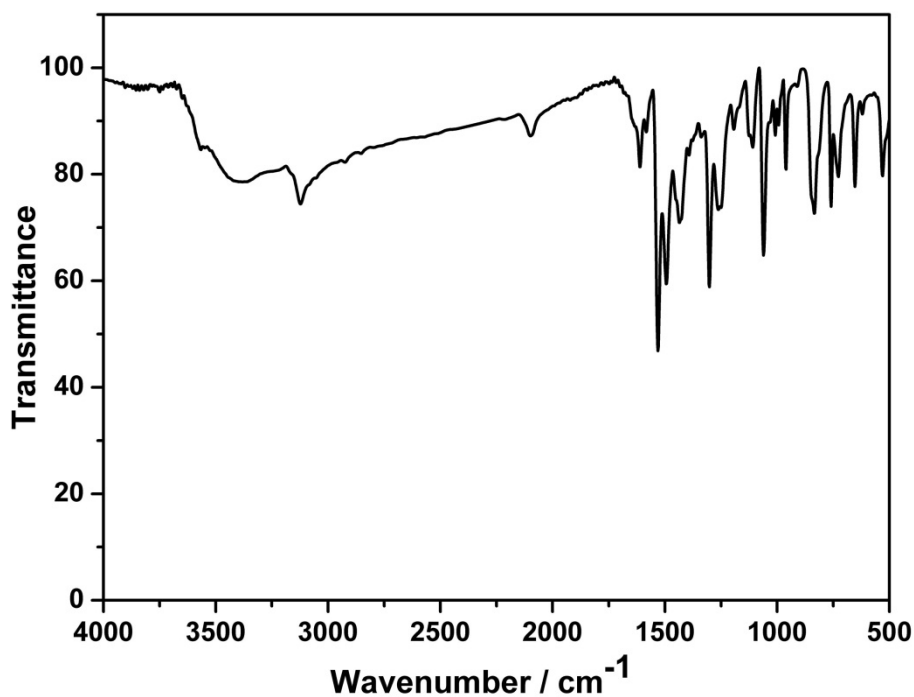
Symmetry transformations used to generate equivalent atoms: #1  $-x-1/2, -y-1/2, z$ ; #2  $-x-1/2, y, z$ ; #3  $-y, -x, -z-1/2$ ; #4  $-x+1/2, y, z$ ; #5  $x, -y-1/2, z$ ; #6  $-x+1/2, -y-1/2, z$ ;



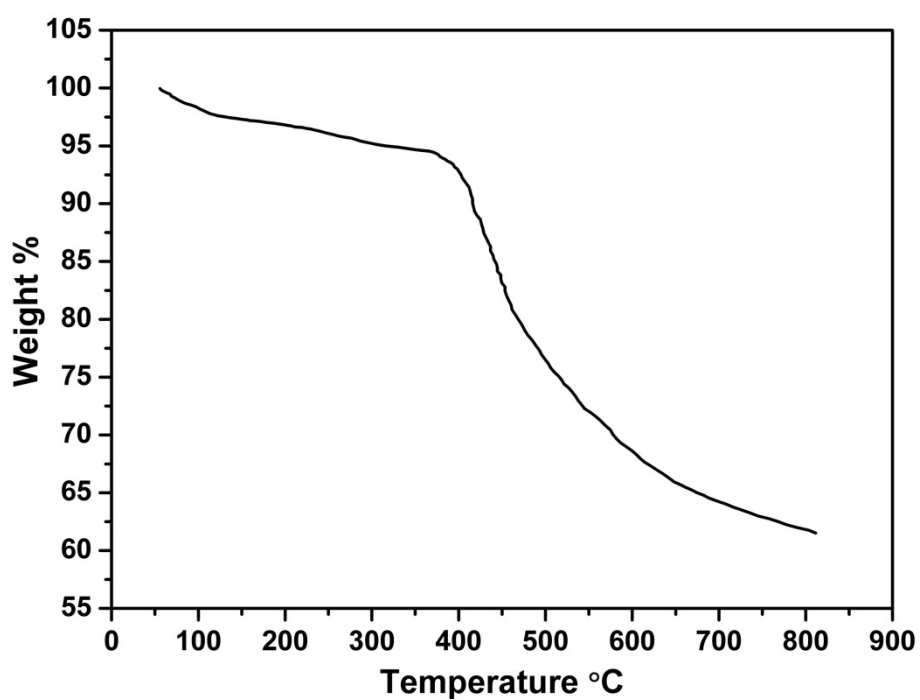


(b)

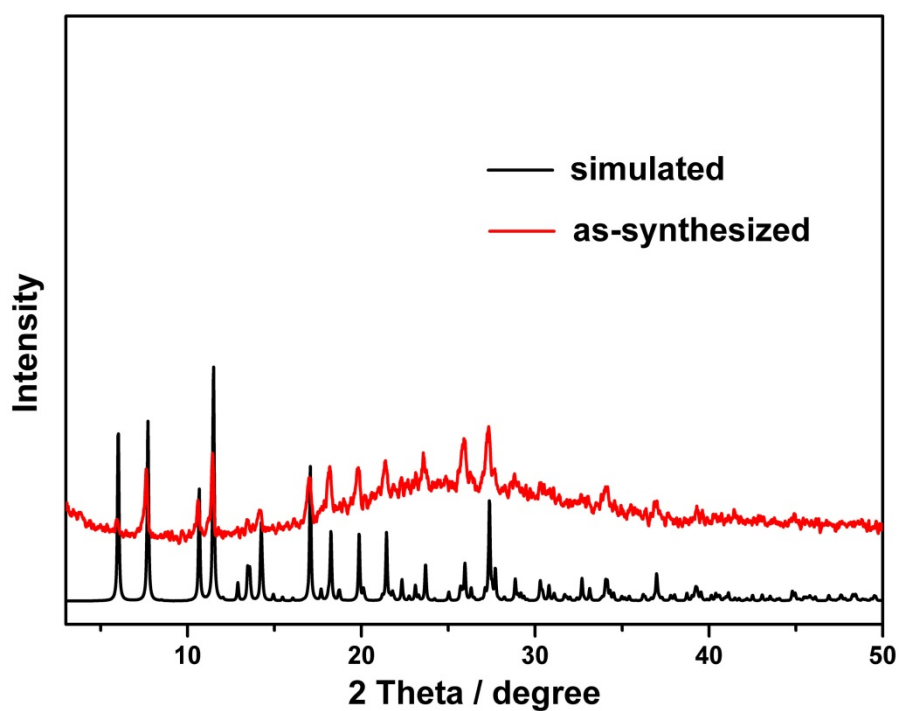
**Figure S1.** (a) XPS spectra for Cu2p<sub>3/2</sub> in compound **1**. In the XPS spectrum of **1**, the peak corresponding to the core-level Cu 2p<sub>3/2</sub> XPS transition is observed at 931.3 eV, and no satellite peak towards a higher binding energy is found which means in **1** all the Cu atoms have the 1+ oxidation state. (b) XPS spectra for Cu2p<sub>3/2</sub> in compound **1** after 90 min of the photocatalytic reaction, which shows all the Cu atoms still have the 1+ oxidation state.



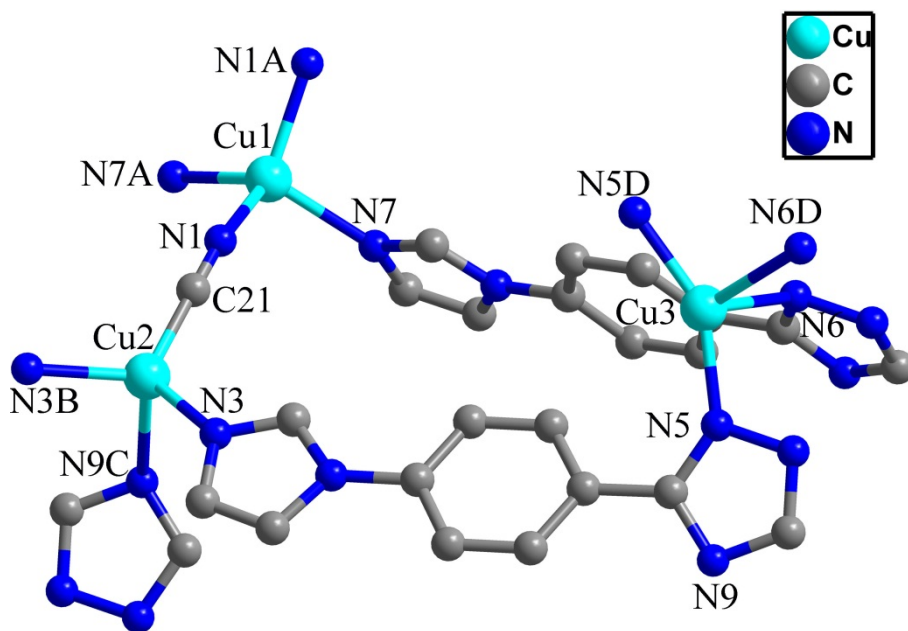
**Figure S2.** Infrared spectrum of fresh **1**.



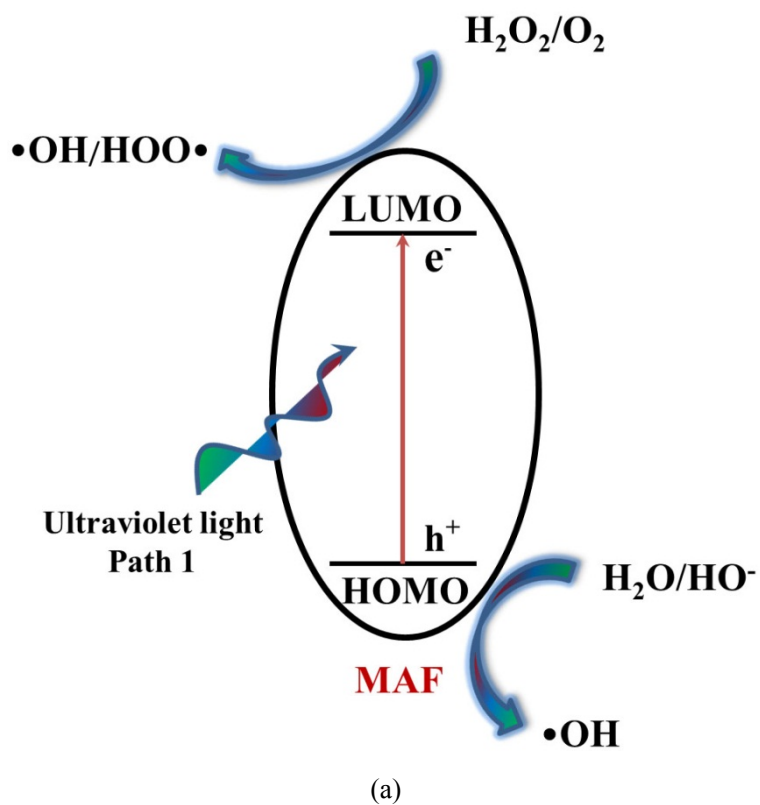
**Figure S3.** TGA curve of compound 1.



**Figure S4.** PXRD profiles of as-synthesized 1 and the simulated one.



**Figure S5.** The coordination environment of Cu1, Cu2 and Cu3 in **1**; Symmetry codes: A:  $-0.5-x, -0.5-y, z$ ; B:  $-0.5-x, y, z$ ; C:  $-0.5+x, y, z$ ; D:  $-y, -x, -0.5-z$ . all the hydrogen atoms have been omitted for clarity.



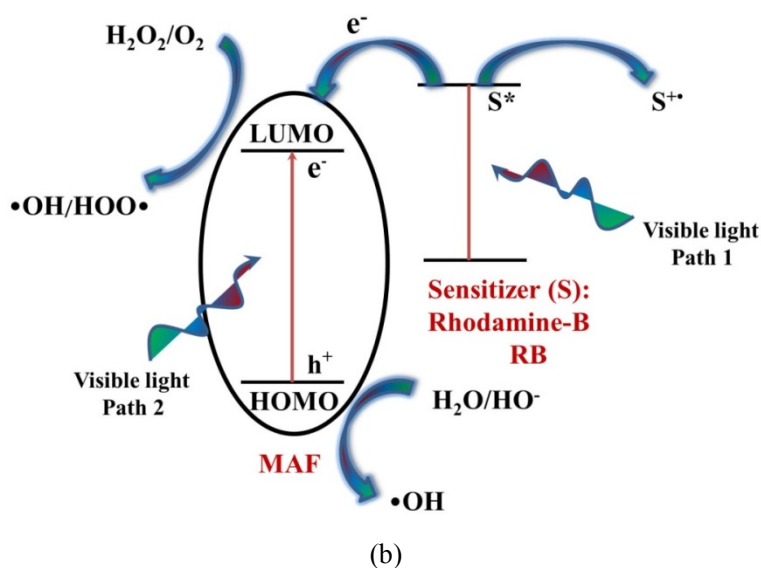


**Figure S6.** (a) Proposed catalytic mechanism of **1** under ultraviolet light irradiation; (b) Proposed catalytic mechanism of **1** under visible light irradiation. In **1**, the HOMO is mainly contributed by nitrogen 2p bonding orbitals (valence band, VB) and the LUMO by empty transition metal orbitals (conduction band, CB). Under ultraviolet light irradiation, electrons ( $e^-$ ) in the HOMO (VB) of MAF were excited to its LUMO (CB), with same amount of holes ( $h^+$ ) left in VB. Then each water molecule adsorbed on the surfaces of **1** provides one electron for the holes in the VB to make it return to its stable state, with the water molecule being oxygenated into  $\bullet\text{OH}$  active species (The holes can also oxidize RB, but the water molecules have better contact with the catalyst surfaces, so finally, the water molecules absorbed on the catalyst surface are oxidized to  $\bullet\text{OH}$ ). Meanwhile, the  $\text{H}_2\text{O}_2$  and oxygen adsorbed on the surface of catalyst **1** can easily trap an electron in the LUMO to form  $\bullet\text{OH}$  and  $\text{O}_2^{\bullet-}$ , respectively. Notably, the attack of  $\text{H}_2\text{O}_2$  by the formed  $\bullet\text{OH}$  radical is one possible way for the formation of superoxide radicals ( $\text{O}_2^{\bullet-}/\text{HOO}\bullet$ ) according to the Haber Weiss mechanism. The formed radicals  $\bullet\text{OH}$  and  $\text{O}_2^{\bullet-}/\text{HOO}\bullet$  attack organic substrates and cleave RB effectively to complete the photocatalytic process. As we know, the degradation of RB is finished through oxidation process, so the electrons ( $e^-$ ) which are excited from the HOMO (VB) of the catalyst to its LUMO (CB) upon light irradiation should be consumed.  $\text{H}_2\text{O}_2$  is added as sacrificial electron acceptor, which is better than other sacrificial electron acceptors because it can easily trap an electron in the LUMO to form  $\bullet\text{OH}$ , one active specie in the degradation of RB. And no harmful substances but water will produce at last. But under the visible light irradiation, the situation is somewhat different. Because RB dye has strong absorption for visible light and its excited state has a rather low redox potential, which means that in our system the RB dye itself can act as the sensitizer. Upon light irradiation, the electron transfer from the dye excited state to the catalyst can occur and the accepted electrons are deposited in the catalyst's LUMO, which can be combined with the oxygen and  $\text{H}_2\text{O}_2$  adsorbed on the surfaces of MAF to form active oxygen species. The remaining process is the same as that under ultraviolet light irradiation.

## References

1. A. Aijaz, P. Lama and P. K. Bharadwaj, *Inorg. Chem.* , 2010, **49**, 5883-5889.
2. G. M. Sheldrick, *SHELXS-97: Program for X-ray crystal structure solution*; , University of Göttingen: Göttingen, Germany, 1997.
3. G. M. Sheldrick, *SHELXL-97: Program for X-ray Crystal Structure Refinement*; , University of Göttingen: Göttingen, Germany, 1997.
4. L. J. Farrugia, *WINGX: A Windows Program for Crystal Structure Analysis*; , University of Glasgow: Glasgow, UK, 1988.